A First Search for Solar ^{8}B Neutrino in the PandaX-4T Experiment using Neutrino-Nucleus Coherent Scattering

Wenbo Ma,[1] Abdusalam Abdukerim,[1] Chen Cheng,[2] Zihao Bo,[1] Wei Chen,[1] Xun Chen,[1,3] Yunhua Chen,[4] Zhaokan Cheng,[5] Xiangyi Cui,[6] Yingjie Fan,[7] Deqing Fang,[8] Changbo Fu,[8] Mengting Fu,[9] Lisheng Geng,[10,11,12] Karl Giboni,[1] Linhui Gu,[1] Xuyuan Guo,[4] Chencheng Han,[6] Ke Han,[1] Changda He,[1] Jinrong He,[4] Di Huang,[1] Yanlin Huang,[13] Zhou Huang,[1] Ruquan Hou,[3] Xiangdong Ji,[14] Yonglin Ju,[15] Chenxiang Li,[1] Jiafu Li,[2] Mingchuan Li,[4] Shu Li,[15] Shuaijie Li,[6] Qing Lin,[16,17,*] Jianglai Liu,[1,6,3,†] Xiaoying Lu,[18,19] Lingyin Luo,[9] Yunyang Luo,[17] Yugang Ma,[8] Yajun Mao,[9] Nasir Shaheed,[18,19] Yue Meng,[1,3,‡] Xuyang Ning,[1] Ningchun Qi,[4] Zhicheng Qian,[1] Xiangxiang Ren,[18,19] Changsong Shang,[4] Xiaofeng Shang,[1] Guofang Shen,[10] Lin Si,[1] Wenliang Sun,[4] Andi Tan,[14] Yi Tao,[1,3] Anqing Wang,[18,19] Meng Wang,[18,19] Qiuhong Wang,[8] Shaobo Wang,[1,20] Siguang Wang,[9] Wei Wang,[5,2] Xiuli Wang,[15] Zhou Wang,[1,3,6] Yuehuan Wei,[5] Mengmeng Wu,[2] Weihao Wu,[1] Jingkai Xia,[1] Mengjiao Xiao,[14] Xiang Xiao,[2] Pengwei Xie,[6] Binbin Yan,[1] Xiyu Yan,[13] Jijun Yang,[1] Yong Yang,[1] Chunxu Yu,[7] Jumin Yuan,[18,19] Ying Yuan,[1] Zhe Yuan,[8] Xinning Zeng,[1] Dan Zhang,[14] Minzhen Zhang,[1] Peng Zhang,[4] Shibo Zhang,[1] Shu Zhang,[2] Tao Zhang,[1] Yingxin Zhang,[18,19] Yuanyuan Zhang,[6] Li Zhao,[1] Qibin Zheng,[13] Jifang Zhou,[4] Ning Zhou,[1] Xiaopeng Zhou,[10] Yong Zhou,[4] and Yubo Zhou[1]

(PandaX Collaboration)

[1]*School of Physics and Astronomy, Shanghai Jiao Tong University, Key Laboratory for Particle Astrophysics and Cosmology (MoE), Shanghai Key Laboratory for Particle Physics and Cosmology, Shanghai 200240, China*
[2]*School of Physics, Sun Yat-Sen University, Guangzhou 510275, China*
[3]*Shanghai Jiao Tong University Sichuan Research Institute, Chengdu 610213, China*
[4]*Yalong River Hydropower Development Company, Ltd., 288 Shuanglin Road, Chengdu 610051, China*
[5]*Sino-French Institute of Nuclear Engineering and Technology, Sun Yat-Sen University, Zhuhai, 519082, China*
[6]*Tsung-Dao Lee Institute, Shanghai Jiao Tong University, Shanghai, 200240, China*
[7]*School of Physics, Nankai University, Tianjin 300071, China*
[8]*Key Laboratory of Nuclear Physics and Ion-beam Application (MOE), Institute of Modern Physics, Fudan University, Shanghai 200433, China*
[9]*School of Physics, Peking University, Beijing 100871, China*
[10]*School of Physics, Beihang University, Beijing 102206, China*
[11]*International Research Center for Nuclei and Particles in the Cosmos & Beijing Key Laboratory of Advanced Nuclear Materials and Physics, Beihang University, Beijing 100191, China*
[12]*School of Physics and Microelectronics, Zhengzhou University, Zhengzhou, Henan 450001, China*
[13]*School of Medical Instrument and Food Engineering, University of Shanghai for Science and Technology, Shanghai 200093, China*
[14]*Department of Physics, University of Maryland, College Park, Maryland 20742, USA*
[15]*School of Mechanical Engineering, Shanghai Jiao Tong University, Shanghai 200240, China*
[16]*State Key Laboratory of Particle Detection and Electronics, University of Science and Technology of China, Hefei 230026, China*
[17]*Department of Modern Physics, University of Science and Technology of China, Hefei 230026, China*
[18]*Research Center for Particle Science and Technology, Institute of Frontier and Interdisciplinary Science, Shandong University, Qingdao 266237, Shandong, China*
[19]*Key Laboratory of Particle Physics and Particle Irradiation of Ministry of Education, Shandong University, Qingdao 266237, Shandong, China*
[20]*SJTU Paris Elite Institute of Technology, Shanghai Jiao Tong University, Shanghai, 200240, China*

(Dated: July 9, 2022)

A search for interactions from solar ^{8}B neutrinos elastically scattering off xenon nuclei using PandaX-4T commissioning data is reported. The energy threshold of this search is further lowered compared to previous search for dark matter, with various techniques utilized to suppress the background that emerges from data with the lowered threshold. A blind analysis is performed on data with an effective exposure of 0.48 tonne·year and no significant excess of events is observed. Among results obtained using neutrino-nucleus coherent scattering, our results give the best constraint on solar ^{8}B neutrino flux. We further provide more stringent limit on cross section between dark matter and nucleon in the mass range from 3 to 10 GeV/c^{2}.

* Corresponding author: qinglin@ustc.edu.cn

† Spokesperson: jianglai.liu@sjtu.edu.cn

‡ Corresponding author: mengyue@sjtu.edu.cn

Due to complex fusion processes inside the Sun, it continuously generate magnificant amount of neutrinos. As liquid xenon (LXe) detectors dedicated to dark matter (DM) direct search [1–3] have been developed into multi-tonne scale in recent years, they are now able to reach the sensitivity to detect solar neutrinos via coherent elastic nuclear scattering (CEνNS). Among all sources of solar neutrinos, neutrinos produced in the β decay of ^{8}B are the most likely ones to be detected due to the 15 MeV Q value. Flux of ^{8}B solar neutrinos on Earth was measured to be approximately 5×10^6 cm^{-2}s^{-1} [4, 5], and its CEνNS has a deposit energy spectrum hardly distinguishable from that of a 6 GeV/c^2 DM particle in LXe. No experimental determination of solar neutrino flux using its CEνNS signal has been made yet. Recently, XENON1T collaboration published a search for the ^{8}B CEνNS signal using 0.6 tonne·year data with no excess found [6]. Due to the low nuclear recoil (NR) energy from ^{8}B CEνNS, it is crucial to lower the energy threshold. In this letter, we report a search for CEνNS induced by solar ^{8}B neutrinos using the commissioning data of PandaX-4T (Run0) based on a blind analysis, with a dedicated data selection, which lowered the 1%-energy-threshold from 1.33 to 0.95 keV.

PandaX-4T dark matter direct search experiment is located in China Jinping underground Laboratory (CJPL) [7, 8]. PandaX-4T experiment utilizes a dual phase xenon time projection chamber (TPC) with a sensitive volume of 3.7 tonne of LXe, and two arrays of photo-multipliers (PMTs) on the top and bottom of the TPC, consisting of 169 and 199 Hamamatsu 3-inch R11410-23 PMTs, respectively. Both the primary scintillation ($S1$) and delayed proportional scintillation from drifted electrons ($S2$) of an event are collected by the PMTs, allowing 3-D position reconstruction with resolution of about a few milimeter on longitudinal and transverse directions, based on the time difference and PMT pattern of the signals, respectively. The waveforms of the PMTs are digitized by CAEN V1725 digitizers and read out under the self-trigger mode when the pulse amplitude is approximately 1/3 photoelectron (PE) above the baseline [9]. More details of detector apparatus can be found in Refs. [9–11]. PandaX-4T has reported the most stringent constraint on spin-independent cross sections between nucleon and weakly interacting massive particles (WIMPs) with mass from 5 GeV/c^2 to 10 TeV/c^2 [10] using the 0.63-tonne-year data from Run0.

Compared to the search reported in Ref. [10], new data selections are developed to enhance the detection efficiency and to minimize the extra background emerged from data. Thresholds of $S1$ and $S2$ are lowered to 0.3 PE and 65 PE, as compared to the 2 PE and 80 PE in Ref. [10]. With this threshold, two sets of data used in Ref. [10] with a total livetime of about 7.5 days show higher noise rate, likely due to micro-discharging in the TPC, and are removed from this analysis. We require selected events having $S2$ widths compatible to expected fluctuation on electron arriving time due to diffusion, and veto PMTs seeing no coincidental photons and no more than 50 PE signals in the event window. These two selections and the fiducial volume (FV) selection of 2.67 tonne are the same as in Ref. [10]. Events with large signals are observed to be followed by small isolated signals in PandaX-4T and other experiments [12, 13]. These isolated signals usually are single electrons (SEs) which have strong correlation with the previous large $S2$ in both time and position. Compared to Ref. [10], a more stringent software veto based on the time and position difference to previous event is implemented. Events with time difference to previous $S2$ (>2000 PE) less than 50 ms or position difference smaller than 100 mm are excluded. In addition, we veto the event unless the total charge per unit time and the number of $S1$s in the preceding 1-ms window return back to normal. We also require that the total charge (in the unit of PEs) in one event waveform (approximately 1 ms) should not exceed $180 + 1.2 \cdot S2_{max}$ where $S2_{max}$ is the largest $S2$ identified in the waveform, the integrated charge is less than 20 PE in the event window before the main S1, and main S1 to be the only signal in a 4-μs window around it, to ensure that the candidate event is not the "afterglow" of a previous event. These selections reduce the effective live time to 64.7 days.

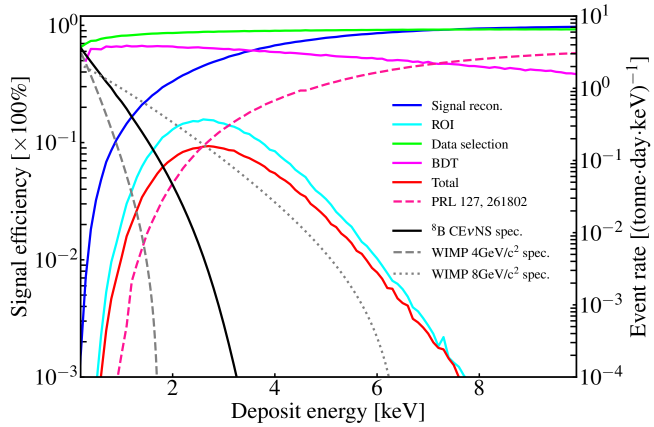

FIG. 1. Total efficiency (red solid lines) to solar ^{8}B neutrino CEνNS in this analysis with number of $S1$ hits to be 2 or 3 hits. The blue, cyan, green, and magenta solid lines represent the signal efficiency caused by signal reconstruction, ROI, data selection, and BDT, respectively. The signal efficiency in previous study [10] is also given in pink dashed line as a reference. The ideal spectra of solar ^{8}B CEνNS and WIMP-nucleus interaction with a WIMP mass of 4 (8) GeV/c^2 with assumed cross section of 10^{-44} cm^2 are overlaid as well in black solid and grey dashed (dotted) curves, respectively, with scales indicated on the right axis.

The total efficiency to ^{8}B CEνNS consists of four components: 1) the efficiency of signal reconstruction, 2) the ROI, 3) data selections, and 4) a cut based on boosted decision tree (BDT, see later text). Signal reconstruction includes clustering of PMT hits into signal pulses, classification of signal pulses into $S1$s and $S2$s, and pairing of the classified $S1$s and $S2$s into incident events. Each step of signal reconstruction is affected by the presence of dark noises and stray electrons. A simulation of signal waveform (WS) is developed to assess the signal reconstruction efficiency. The simulated $S1$s in WS for nuclear recoil (NR) signals (^{8}B CEνNS and WIMP signals, see next paragraph) are sampled from waveforms of $S1$ hits from neutron calibration data, similar to what was done in Ref. [14]. The $S2$s at a given position (X, Y) are simulated by assembling SE waveforms from the data, with reconstructed position within a 40-mm radius circle (tuned to match the data). The width of the overall assembled waveform at a given depth in the TPC is required to satisfy the diffusion relation observed from data. Effects of PMT afterpulsing, delayed electrons [13, 15–17], and photo-ionziation of impurities after a large $S2$ are implemented in the WS according to the data. The efficiency of the signal reconstruction is shown in Fig. 1. For the ROI, we require the number of coincident PMT hits in an $S1$ to be either 2 or 3 in this analysis. Events with $S1$ hit number of 1 are mostly accidental background originated from PMT dark noises, and are excluded from the ROI due to a poor signal-to-background ratio. The $S2$ charge range, uncorrected for spatial dependence, is further optimized and will be described in later text. This ROI requirement has dominating effects on the signal efficiency, as shown in Fig. 1. The efficiency of data selections are estimated through the WS (see Fig. 1) and validated by $S2$s from neutron calibration and surface events with their difference taken as the systematic uncertainty. The difference between efficiencies using the WS, NR calibration and surface event samples is taken as the systematic uncertainty.

We take the calculated deposit energy spectrum of solar ^{8}B CEνNS in LXe from Ref. [18], which is shown in Fig. 1 along with deposit energy spectra of WIMP with mass of 4 and 8 GeV/c^2. The signal model implements the light and charge production in LXe following the NEST v2.3.6 parametrization [19], and the response of signal detection in PandaX-4T detector, similar to Ref. [10]. The light and charge yields are extrapolated from the one used in Ref. [10], which has its model parameters fit to the neutron calibration data in the energy region of WIMP search (see Fig. 2). We adopt the relative uncertainties of light and charge yields from NEST [20], which is based on a global fit to all available measurements, and conservatively assume them to be uncorrelated.

The background composition is the same as Ref. [10]. With loosened $S1$ and $S2$ selections, the accidental coincidence (AC) background increases significantly in comparison to Ref. [10], which dominates the overall background. The ER and NR background is estimated using the same method as in Ref. [10] but with the new data selections and the ROI cut. The surface background is negligible.

The AC background is constructed from data waveforms. The random $S2$s are selected after physical $S1$s

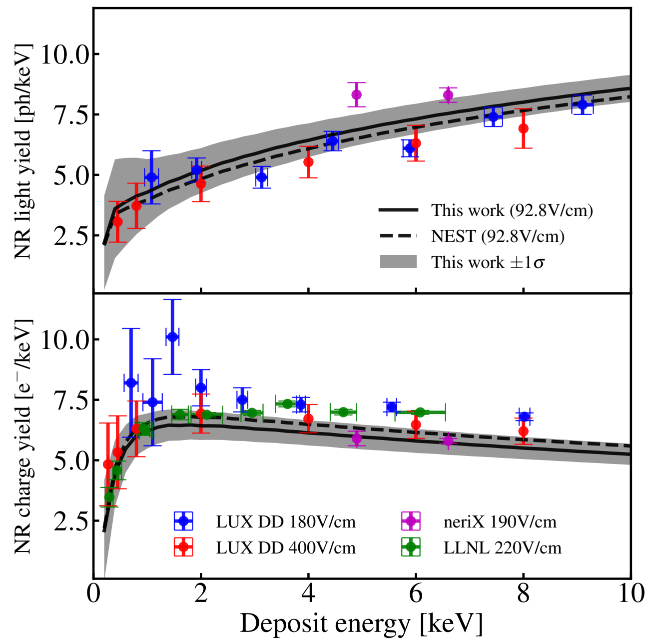

FIG. 2. Comparison between light (top panel) and charge (bottom panel) yields used in this analysis (in solid black lines) with nominal NEST v2.3.6 [19] (shown in dashed black lines) and other measurements taken at different drift electric fields [21–24]. The 1σ uncertainty from Ref. [20] for light and charge yields are shown in black shaded regions.

in a off-window of [0.9, 1.5] ms, beyond the TPC's maximum drift time. The rate of uncorrelated $S2$ within 65 to 300 PE after all data selection cuts is estimated to be about 1000 per day. The waveform of such $S2$ is concatenated after a 1 ms segment randomly selected from our recorded data, which on average contains 6.3 (0.01) of $S1$-like signals with $S1$ hit equals to (larger than) 1, primarily from dark noises. This "scrambled" waveform data form the basis of the AC estimate, which then get passed to the aforementioned software reconstruction and data selection. Under this procedure, the overall AC rate is anchored by the random $S2$ rate derived from the off-window. The predicted number of AC in the ROI in 2- and 3-hit regions can be found in Table I. The diffusion cut is the most effective cut, which suppresses the AC by a factor of 8 or so. The AC model is validated using events with $S2$ in the range from 300 to 800 PE (referred to as the side-band data) and within the FV, which is dominated by AC particularly for the 1-hit region (see Table II). The comparison between side-band data and the prediction is given in Table II, and the agreement in rate is excellent. The comparison between the $S1$ and $S2$ spectra of the prediction and side-band data is shown in Fig. 3. To be conservative, we take 30%, which is the difference (error-weighted standard deviation) in the normalized $S2$ spectra, as the systematic uncertainty of the AC model.

The $S2$s of AC are mostly generated out of the fiducial

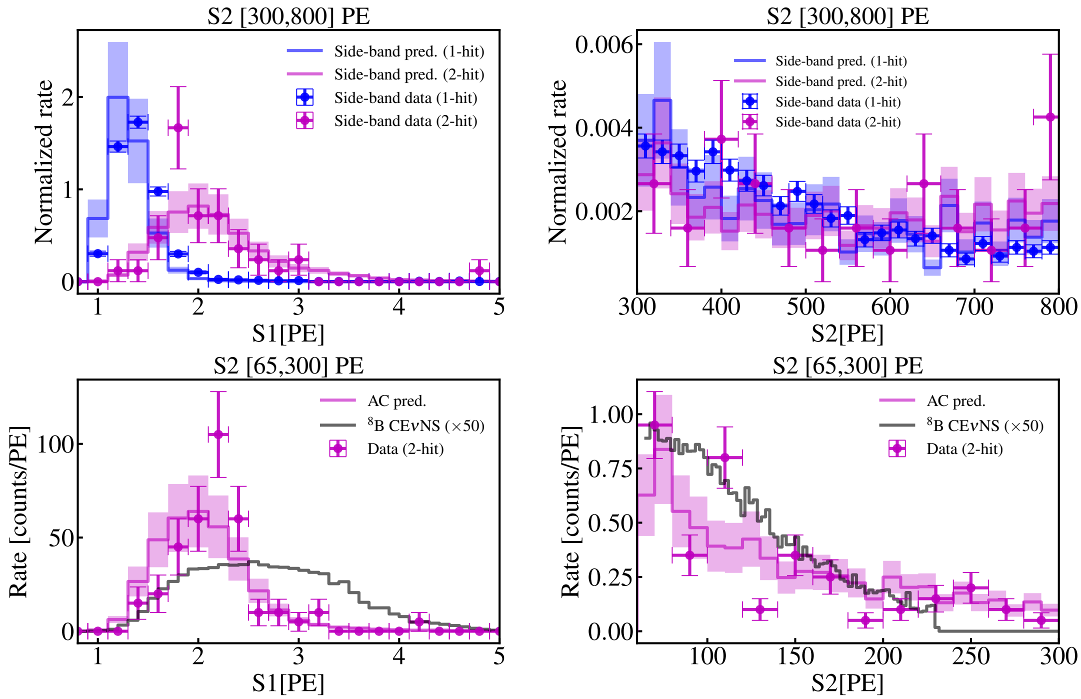

FIG. 3. The $S1$ (left panels) and $S2$ (right panels) spectra in the side-band (top panels) and ROI (bottom panels), with data and corresponding predictions overlaid. Shaded regions represent the 1σ uncertainty of the prediction. We also overlay the expected ^{8}B CEνNS spectra (scaled up by 50) in bottom panels, shown in black solid lines.

TABLE I. The expected number of solar ^{8}B neutrino CEνNS events and background events (including the ER, neutron and AC background) after all data selections in the optimized $S2$ ranges. The observed numbers are given in the last column. Number of events before and after the BDT cuts are shown in separate rows. .

N_{hit}	$S2$ range	BDT	ER	NR	AC	Total bkg	^{8}B	Obs.
2	65-230 PE	off	0.04	0.10	62.43	62.57	2.32	**59**
		on	0.00	0.04	1.41	1.46	1.42	**1**
3	65-190 PE	off	0.01	0.05	0.79	0.85	0.42	**2**
		on	0.00	0.02	0.02	0.04	0.29	**0**

TABLE II. Comparison between AC predictions N_{AC}, physical event prediction N_{phys}, and the data N_{obs} in side-band region.

N_{hit}	Side-band		
	N_{phys}	N_{AC}	N_{obs}
1	9.4	2060.5	2043
2	10.1	33.8	47
3	6.9	6.9	7

region (such as surface of electrodes and gas region), and $S1$s are mostly dark noises (see Ref. [25]). A boosted decision tree (BDT) algorithm [26] is trained to optimize the ^{8}B CEνNS selection against the AC background. The input variables of the BDT concern features related to the charge, width, top-bottom asymmetry and PMT top patterns of the $S1$ and $S2$ signals. The training and testing samples of ^{8}B signal in the BDT are from the WS with ($S1$, $S2$) distribution following our ^{8}B signal model. The BDT cut value and the $S2$ range for each $S1$ hit bin are determined by maximizing the probability of discovering a ^{8}B signal under our background model, with results summarized in Table I. The optimized BDT efficiency of ^{8}B signal is shown in Fig. 1. The BDT reduces the ^{8}B CEνNS signal (AC background) by about 39% (98%) and 31% (96%), respectively, for the 2- and 3-hit bins. Most of the rejection power against AC is gained through parameters related to the $S2$ waveform shape and its top charge pattern. The systematic uncertainty of the rejection power of the BDT against AC background is estimated by checking the performances on an alternative AC model using more traditional approach based on random pairing of isolated $S1$s and $S2$s [25], leading to an approximately 19% uncertainty to the reduced background. The uncertainty of the BDT efficiency to signal is studied using neutron data. A difference of 26% and 23% are observed for the 2-hit and 3-hit ROI, respectively, and we assign them as the systematic uncertainty. The larger systematic uncertainty on NR data could be originated from the imperfection of NR modeling in the WS.

The data within the ROI were blinded before we finalized the data selection, background and signal models, ROI, and BDT optimization. We then unblind the data

TABLE III. List of constrained nuisance parameters that are included in the final statistical interpretation (see text), along with the means and standard deviations of their Gaussian constraints.

	Description	mean of G	std. of G 2-hit	std. of G 3-hit
η_{mod}	NEST model scaling	0	1	
η_{AC}	AC sample scaling	1	0.30	
η_{cut}	Data selection eff. scaling	1	0.04	
η_{flux}	^{8}B flux scaling [5]	1	0.04	
$\theta_{i,\mathrm{BDT}_s}$	BDT scaling for signal	1	0.26	0.23
$\theta_{i,\mathrm{BDT}_{\mathrm{AC}}}$	BDT scaling for AC	1	0.19	0.18

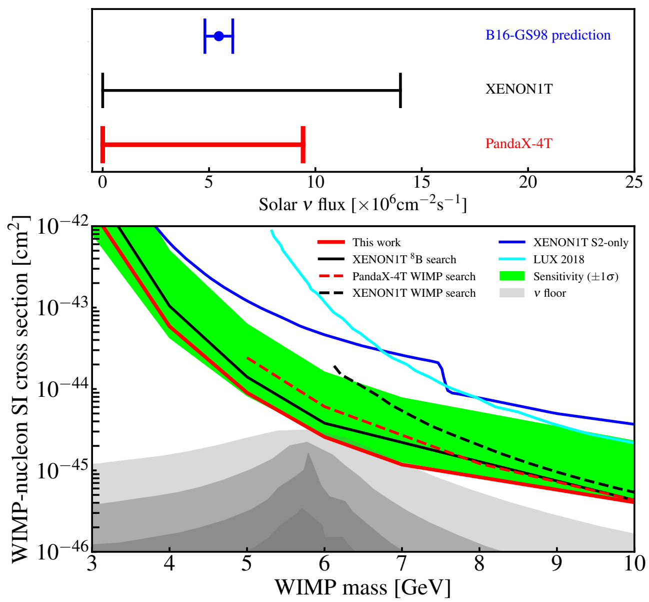

FIG. 4. Top panel: our constraint on solar neutrino flux using CEνNS analysis, along with XENON1T results [6] using the same CEνNS detection channel and B16-GS98 standard solar model prediction [30]. Bottom panel: updated constraints on WIMP-nucleon spin-independent cross section. The red solid and dashed line represents the results from this and previous searches [10], respectively. The black solid and dashed lines represent the results from XENON1T with and without optimization in the low-energy region [6, 27]. Several results from other experiments [28, 29] are also shown. The neutrino floors (probability for an ideal xenon detector to see less-than-3σ-significance DM signal) [18] under different exposure assumptions (1, 10, 100, and 1000 tonne-year from top to bottom) are shown in grey shaded regions. The green and yellow shaded region represents the $\pm 1\sigma$ region of sensitivity for the WIMP search.

and check the events before and after the BDT applied. We show the comparison of $S1$ and $S2$ spectra between the prediction and data before the BDT in Fig. 3. The observed number of events in the ROI for 2- and 3-hit regions are given in Table I. After unblinding, 1 (with $S1$=1.6 PE and $S2$=165 PE) and 0 events are found in 2- and 3-hit ROI that survive the BDT.

We perform a simple statistical interpretation based on 2-bin profile likelihood ratio (PLR) analysis (following definition in Ref. [31]) using the 2- and 3-hit data. The binned likelihood is defined as:

$$\mathcal{L} = G(\boldsymbol{\eta}) \prod_i \frac{\lambda_i^{N_i}}{N_i!} e^{-\lambda_i} \cdot G(\boldsymbol{\theta_i}), \tag{1}$$

where the index i represents the hit number of $S1$ (2 or 3), and $\boldsymbol{\eta}$ ($\boldsymbol{\theta_i}$) is series of constrained nuisance parameters, which are correlated (independent) between 2- and 3-hit bins with a Gaussian penalty G. The set of parameters include η_{mod}, η_{AC}, η_{cut}, η_{flux}, $\theta_{i,\mathrm{BDT}_s}$, and $\theta_{i,\mathrm{BDT}_{\mathrm{AC}}}$, corresponding to the uncertainties of LXe light/charge model, AC background, ^{8}B neutrino flux, the BDT cut for signals, and the BDT cut for the AC background, respectively, with their means and 1σ values summarized in Table III. λ_i is the expected count while N_i is the observed count. The expected counts for the low-mass WIMP search and for ^{8}B CEνNS in the signal+background hypothesis can be written as:

$$\begin{aligned}
\lambda_i^{\chi} =&(1+f_i^{\chi}\eta_{\mathrm{mod}})\eta_{\mathrm{cut}}\theta_{i,\mathrm{BDT}_s} \cdot N_{\mathrm{wimp}} \\
&+ (1+f_i^{\nu}\eta_{\mathrm{mod}})\eta_{\mathrm{cut}}\theta_{i,\mathrm{BDT}_s}\eta_{\mathrm{flux}} \cdot N_{\nu} \\
&+ \eta_{\mathrm{cut}} \cdot \theta_{i,\mathrm{BDT}_{\mathrm{AC}}} \cdot \eta_{\mathrm{AC}} \cdot N_{\mathrm{AC}} + N_{\mathrm{other}}, \\
\lambda_i^{\nu} =&(1+f_i^{\nu}\eta_{\mathrm{mod}})\eta_{\mathrm{cut}}\theta_{i,\mathrm{BDT}_s} \cdot N_{\nu} \\
&+ \eta_{\mathrm{cut}} \cdot \theta_{i,\mathrm{BDT}_{\mathrm{AC}}} \cdot \eta_{\mathrm{AC}} \cdot N_{\mathrm{AC}} + N_{\mathrm{other}},
\end{aligned} \tag{2}$$

where λ_i^{χ} and λ_i^{ν} are the expected count in the two hypotheses. N_{wimp}, N_{ν}, N_{AC}, and N_{other} are the expected number of counts for low-mass WIMP, ^{8}B CEνNS, AC, and other background events (including ER and neutron), respectively. f_i is the fractional uncertainty to signal rates due to uncertainties in the light and charge yields, and depends on energy spectrum of interpreted signal. Typical numbers of f_i are 0.45 (0.60), 0.29 (0.39), and 0.19 (0.30) for 4-GeV/c^2 WIMP, ^{8}B CEνNS, and 7-GeV/c^2 WIMP in 2-hit (3-hit) region. The total backgrounds predicted in the 2- and 3-hit ROI for solar ^{8}B neutrino search are 1.46 and 0.04, respectively, in an exposure of 0.48 tonne·year, as shown in Table I. Uncertainty for other background events is negligible and ignored here. The observed number of events is consistent with two background-only hypotheses in searching for a) solar ^{8}B neutrino CEνNS without WIMP, and b) low mass WIMP with nominal ^{8}B CEvNS background, representing a probability of 56% and 20% of observing the same or less number of events than the data, respectively.

Using a similar procedure as in Refs. [10, 31], we give the 90% upper limit on solar ^{8}B neutrino flux using the CEνNS channel, pushing the upper limit to 9.4×10^6/cm^2/s, in comparison to $(5.46\pm0.66)\times10^6$/cm^2/s from the standard solar model B16-GS98 [30]. Under the nominal ^{8}B CEvNS rate, we also obtain the best constraints on the spin-independent WIMP-nucleon cross section with mass in the range of 3 to 10 GeV/c^2. The results are summarized in Fig. 4. In Fig. 4, we also show the ^{8}B neutrino floor curves from Ref. [18] under ideal background assumption. The current stage of PandaX has clearly entered into the sensitive region, so this result could also be cast into interesting parameter space of neutrino interactions. The lack of CEvNS excess from this work and XENON1T [6] also suggest further investigations on the response of LXe TPC to ultralow energy nuclear recoils.

In summary, a search for CEνNS from solar ^{8}B neutrinos as well as low mass WIMP-nucleon interactions are performed using the PandaX-4T commissioning data with 0.48 tonne·year exposure. In the analysis, we have further optimized the data selection, and developed various techniques to lower the energy threshold and to control the accidental background. No significant excess is observed, leading to the strongest upper limit on solar ^{8}B neutrino flux using CEvNS, and on the spin-independent WIMP-nucleon cross section within the mass range from 3 to 10 GeV/c^2. This manifests the potential of PandaX-4T as a highly sensitive multi-purpose dark matter and astrophysical neutrino observatory.

This project is supported in part by Office of Science and Technology, Shanghai Municipal Government (grant No. 18JC1410200), a grant from the Ministry of Science and Technology of China (No. 2016YFA0400301), and grants from National Science Foundation of China (Nos. 12005131, 11905128, 12090061, 11775141). We thank supports from Double First Class Plan of the Shanghai Jiao Tong University. We also thank the sponsorship from the Chinese Academy of Sciences Center for Excellence in Particle Physics (CCEPP), Hongwen Foundation in Hong Kong, and Tencent Foundation in China. Finally, we thank the CJPL administration and the Yalong River Hydropower Development Company Ltd. for indispensable logistical support and other help.

[1] E. Aprile, J. Aalbers, F. Agostini, M. Alfonsi, L. Althueser, F. Amaro, V. C. Antochi, E. Angelino, J. Angevaare, F. Arneodo, et al., Projected wimp sensitivity of the xenonnt dark matter experiment, Journal of Cosmology and Astroparticle Physics **2020** (11), 031.

[2] D. Akerib, C. Akerlof, S. Alsum, H. Araújo, M. Arthurs, X. Bai, A. Bailey, J. Balajthy, S. Balashov, D. Bauer, et al., Projected wimp sensitivity of the lux-zeplin dark matter experiment, Physical Review D **101**, 052002 (2020).

[3] H. Zhang, A. Abdukerim, W. Chen, X. Chen, Y. Chen, X. Cui, B. Dong, D. Fang, C. Fu, K. Giboni, et al., Dark matter direct search sensitivity of the pandax-4t experiment, Science China Physics, Mechanics & Astronomy **62**, 1 (2019).

[4] M. Agostini, K. Altenmüller, S. Appel, D. Jeschke, B. Neumair, L. Oberauer, L. Papp, S. Schönert, F. von Feilitzsch, V. Atroshchenko, et al., Comprehensive measurement of pp-chain solar neutrinos, Nature **562**, 505 (2018).

[5] B. Aharmim, S. Ahmed, A. Anthony, N. Barros, E. Beier, A. Bellerive, B. Beltran, M. Bergevin, S. Biller, K. Boudjemline, et al., Combined analysis of all three phases of solar neutrino data from the sudbury neutrino observatory, Physical Review C **88**, 025501 (2013).

[6] E. Aprile, J. Aalbers, F. Agostini, S. A. Maouloud, M. Alfonsi, L. Althueser, F. Amaro, S. Andaloro, V. C. Antochi, E. Angelino, et al., Search for coherent elastic scattering of solar b 8 neutrinos in the xenon1t dark matter experiment, Physical review letters **126**, 091301 (2021).

[7] K.-J. Kang, J.-P. Cheng, Y.-H. Chen, Y. Li, M. Shen, S. Wu, and Q. Yue, Status and prospects of a deep underground laboratory in china, in Journal of Physics: Conference Series, Vol. 203 (IOP Publishing, 2010) p. 012028.

[8] J. Li, X. Ji, W. Haxton, and J. S. Wang, The second-phase development of the china jinping underground laboratory, Physics Procedia **61**, 576 (2015).

[9] C. He, J. Liu, X. Ren, X. Shang, X. Wei, M. Wang, J. Yang, Y. Yang, G. Zhang, and Q. Zheng, A 500 ms/s waveform digitizer for pandax dark matter experiments, Journal of Instrumentation **16** (12), T12015.

[10] Y. Meng, Z. Wang, Y. Tao, A. Abdukerim, Z. Bo, W. Chen, X. Chen, Y. Chen, C. Cheng, Y. Cheng, et al., Dark matter search results from the pandax-4t commissioning run, Physical review letters **127**, 261802 (2021).

[11] L. Zhao, X. Cui, W. Ma, Y. Fan, K. Giboni, T. Zhang, J. Liu, and X. Ji, The cryogenics and xenon handling system for the pandax-4t experiment, Journal of Instrumentation **16** (06), T06007.

[12] E. Aprile et al. (XENON100), Observation and applications of single-electron charge signals in the xenon100 experiment, Journal of Physics G: Nuclear and Particle Physics **41**, 035201 (2014).

[13] D. Akerib, S. Alsum, H. Araújo, X. Bai, J. Balajthy, A. Baxter, E. Bernard, A. Bernstein, T. Biesiadzinski, E. Boulton, et al., Investigation of background electron emission in the lux detector, Physical Review D **102**, 092004 (2020).

[14] D. Akerib, C. Akerlof, A. Alqahtani, S. Alsum, T. Anderson, N. Angelides, H. Araújo, J. Armstrong, M. Arthurs, X. Bai, et al., Simulations of events for the lux-zeplin (lz) dark matter experiment, Astroparticle Physics **125**, 102480 (2021).

[15] P. Sorensen and K. Kamdin, Two distinct components of the delayed single electron background signals in liquid xenon emission detectors, arXiv preprint arXiv:1711.07025 (2017).

[16] P. Sorensen, Electron train backgrounds in liquid xenon dark matter search detectors are indeed due to thermalization and trapping, arXiv preprint arXiv:1702.04805 (2017).

[17] D. Akerib, S. Alsum, H. Araújo, X. Bai, J. Balajthy, J. Bang, A. Baxter, E. Bernard, A. Bernstein, T. Biesiadzinski, et al., Improving sensitivity to low-mass dark matter in lux using a novel electrode background mitigation technique, Physical Review D **104**, 012011 (2021).

[18] F. Ruppin, J. Billard, E. Figueroa-Feliciano, and L. Strigari, Complementarity of dark matter detectors in light of the neutrino background, Physical Review D **90**, 083510 (2014).

[19] M. Szydagis, J. Balajthy, J. Brodsky, J. Cutter, J. Huang,

E. Kozlova, B. Lenardo, A. Manalaysay, D. McKinsey, M. Mooney, et al., Noble element simulation technique v2. 0, Zenodo: Geneve, Switzerland (2018).

[20] M. Szydagis, The noble element simulation technique (nest): Recent updates and improvements, Bulletin of the American Physical Society (2022).

[21] D. Akerib, S. Alsum, H. Araújo, X. Bai, A. Bailey, J. Balajthy, P. Beltrame, E. Bernard, A. Bernstein, T. Biesiadzinski, et al., Low-energy (0.7-74 kev) nuclear recoil calibration of the lux dark matter experiment using dd neutron scattering kinematics, arXiv preprint arXiv:1608.05381 (2016).

[22] D. Huang, Ultra-low energy calibration of the lux and lz dark matter detectors, Ph. D. Thesis (2020).

[23] E. Aprile, M. Anthony, Q. Lin, Z. Greene, P. de Perio, F. Gao, J. Howlett, G. Plante, Y. Zhang, and T. Zhu, Simultaneous measurement of the light and charge response of liquid xenon to low-energy nuclear recoils at multiple electric fields, Physical Review D **98**, 112003 (2018).

[24] B. Lenardo, J. Xu, S. Pereverzev, O. A. Akindele, D. Naim, J. Kingston, A. Bernstein, K. Kazkaz, M. Tripathi, C. Awe, et al., Measurement of the ionization yield from nuclear recoils in liquid xenon between 0.3–6 kev with single-ionization-electron sensitivity, arXiv preprint arXiv:1908.00518 (2019).

[25] A. Abdukerim, W. Chen, X. Chen, Y. Chen, C. Cheng, X. Cui, Y. Fan, D. Fang, C. Fu, M. Fu, et al., Study of background from accidental coincidence signals in the pandax-ii experiment, arXiv preprint arXiv:2204.11175 (2022).

[26] A. Hoecker, P. Speckmayer, J. Stelzer, J. Therhaag, E. von Toerne, H. Voss, M. Backes, T. Carli, O. Cohen, A. Christov, et al., Tmva-toolkit for multivariate data analysis, arXiv preprint physics/0703039 (2007).

[27] E. Aprile, J. Aalbers, F. Agostini, M. Alfonsi, L. Althueser, F. Amaro, M. Anthony, F. Arneodo, L. Baudis, B. Bauermeister, et al., Dark matter search results from a one tonne × year exposure of xenon1t, arXiv preprint arXiv:1805.12562 (2018).

[28] E. Aprile, J. Aalbers, F. Agostini, M. Alfonsi, L. Althueser, F. Amaro, V. C. Antochi, E. Angelino, F. Arneodo, D. Barge, et al., Light dark matter search with ionization signals in xenon1t, Physical Review Letters **123**, 251801 (2019).

[29] D. Akerib, S. Alsum, H. Araújo, X. Bai, A. Bailey, J. Balajthy, P. Beltrame, E. Bernard, A. Bernstein, T. Biesiadzinski, et al., Results from a search for dark matter in the complete lux exposure, Physical review letters **118**, 021303 (2017).

[30] N. Vinyoles, A. M. Serenelli, F. L. Villante, S. Basu, J. Bergström, M. Gonzalez-Garcia, M. Maltoni, C. Peña-Garay, and N. Song, A new generation of standard solar models, The Astrophysical Journal **835**, 202 (2017).

[31] D. Baxter, I. Bloch, E. Bodnia, X. Chen, J. Conrad, P. Di Gangi, J. Dobson, D. Durnford, S. Haselschwardt, A. Kaboth, et al., Recommended conventions for reporting results from direct dark matter searches, The European Physical Journal C **81**, 1 (2021).